Biochemistry

 Volume 41, Number 3 January 22, 2002

Current Topics

Biological and Chemical Applications of Fluorescence Correlation Spectroscopy: A Review†

Samuel T. Hess,‡,§ Shaohui Huang,§,|| Ahmed A. Heikal,§,|| and Watt W. Webb*,||

Department of Physics and School of Applied and Engineering Physics, Clark Hall, Cornell University, Ithaca, New York 14853

Received September 26, 2001; Revised Manuscript Received November 1, 2001

I. HISTORICAL PERSPECTIVE

The mathematical concept of fluorescence correlation spectroscopy (FCS)[1] (*1*) emerged from quasi-elastic light scattering (QELS) spectroscopy (*2*) in the early 1970s. Compared to light scattering, the enhanced sensitivity of fluorescence to changes in molecular structure, chemistry, and local environment makes FCS a superior analytical tool for chemical kinetics studies (*1*, *3*−*5*).

The primary motivation for the invention of FCS was the study of chemical kinetics at very dilute concentrations in biological systems, such as the reversible binding reaction between ethidium bromide, a fluorescent nucleic acid synthesis inhibitor, and DNA (*1*). Theoretical and experimental studies (*3*, *4*, *6*) soon established that FCS could measure not only diffusion coefficients but also chemical rate constants, concentration, aggregation, and rotational dynamics (*3*−*9*). Building on this foundation, significant advances in the understanding of lipid diffusion in membranes were made soon after the birth of FCS (*10*) using a confocal microscope geometry (*11*) introduced into FCS by Koppel et al. (*7*) and still used today.

Recently, technological advances in detectors, autocorrelation electronics, and confocal microscopy were incorporated into FCS, mainly in the laboratories of R. Rigler and M. Eigen (*12*, *13*). A detailed theoretical framework on the effects of translational and rotational motion of a fluorescent molecule undergoing chemical reactions, in a three-dimensional (3D) Gaussian observation volume, has been introduced (*14*). Statistical analysis provided the basis for optimizing the signal-to-noise ratio (S/N) in FCS (*15*). Furthermore, analytic functions describing molecular translation (*16*), shot noise effects on higher-order fluorescence fluctuation moments (*17*), and the effect of the observation volume (*18*) on the S/N were explored. Finally, the ability of FCS to resolve multiple species with equivalent diffusion properties was extended by probability analysis of fluorescence intensity distributions (*19*−*22*). These advances extend the horizon of FCS in biological and chemical studies (for a recent review, see ref *23*).

II. THEORETICAL BACKGROUND

The fluorescence (or concentration) fluctuations of a molecular system are the key observable in FCS. Fluorescence fluctuations are autocorrelated to quantify the temporal

† This work was supported by National Institutes of Health (NIH) Grant P41-2RR04224 and National Science Foundation (NSF) Grants DBI-0080792 and 9419978, and carried out in the NIH-NCRR-supported Developmental Resource for Biophysical Imaging Optoelectronics. S.T.H. benefited from an NSF Graduate Research Fellowship and an NIH Molecular Biophysics Training Grant (GM08267).

* To whom correspondence should be addressed. Phone: (607) 255-3331. Fax: (607) 255-7658. E-mail: www2@cornell.edu.

‡ Department of Physics.

§ These authors contributed equally to this work.

|| School of Applied and Engineering Physics.

[1] Abbreviations: FCS, fluorescence correlation spectroscopy; QELS, quasi-elastic light scattering; FPR, fluorescence photobleaching recovery; 3D, three-dimensional; S/N, signal-to-noise ratio; 2D, two-dimensional; 2PE, two-photon excitation; 1PE, one-photon excitation; GFP, green fluorescent protein; IFP, intrinsically fluorescent protein; dsRed, *Discosoma* Red; FRET, fluorescence resonance energy transfer; CD, circular dichroism; PCR, polymerase chain reaction; HIV-1, human immunodeficiency virus-1; BLMs, planar lipid bilayers; TRFA, time-resolved fluorescence anisotropy; PCH, photon counting histogram; FIDA, fluorescence intensity distribution analysis; NADH, nicotinamide adenine dinucleotide; GUVs, giant unilamellar vesicles; NA, numerical aperture; HTS, high-throughput screening.

10.1021/bi0118512 CCC: $22.00
Published on Web 12/20/2001

evolution of the system about its equilibrium state, thereby revealing nonequilibrium properties based on the Onsager hypothesis (*24*) and the fluctuation dissipation theorem. For a single molecular species, the temporal evolution of concentration fluctuations can be quantified via the corresponding fluctuations $\delta F(t)$ in the fluorescence signal $F(t)$ around its mean value $\langle F(t)\rangle$, where $\delta F(t) = F(t) - \langle F(t)\rangle$, and t is time. For a more mathematical introduction, see refs *13*, *23*, and *25*. The normalized autocorrelation function $G(\tau)$ of a fluorescence fluctuation at a given time, $\delta F(t)$, and at a later time $\delta F(t + \tau)$, is then given by the equation $G(\tau) = \langle \delta F(t)\ \delta F(t + \tau)\rangle / \langle F(t)\rangle^2$. Thus, $G(\tau)$ contains information about concentration fluctuations of observed molecules, reflecting the molecular dynamics of the system.

II.A. Single Diffusing Species in a Gaussian Observation Volume without Chemical Kinetics. For a single diffusing species, concentration fluctuations in an open observation volume are caused by diffusion of molecules through this volume. In a confocal microscope configuration, the observation volume is defined as the convolution of the spatial excitation and detection volumes, which depend on laser wavelength, objective specifications, and confocal detector aperture (*13*, *14*, *26*). In multiphoton FCS, the confocal aperture becomes unnecessary and the observation volume is defined exclusively by the excitation intensity profile (*27*).

In the standard case of an assumed prolate ellipsoidal Gaussian observation volume in the absence of chemical kinetics, the autocorrelation function has the following analytical form (*12*, *14*):

$$G_D(\tau) = 1/[N(1 + \tau/\tau_D)(1 + \tau/\omega^2\tau_D)^{0.5}] \qquad (1)$$

where τ_D is the characteristic diffusion time during which a molecule resides in the observation volume with an axial (z_0) to lateral (r_0) dimension ratio ω ($=z_0/r_0$). In the limit $\tau \rightarrow 0$, the mean number of fluorescent molecules N, at concentration C, can be calculated from the initial correlation amplitude, $G_D(\tau \rightarrow 0) = 1/N = 1/CV$, in a defined observation volume V. Fluorescence fluctuations from a given molecule correlate with themselves but not with those from other (independent) molecules. As the number of molecules in the observation volume grows, the relative effect of a single molecule on the total fluorescence signal decreases and, thus, the normalized autocorrelation amplitude decreases. This intuitively explains the inverse relationship of $G_D(\tau)$ with the total number of molecules in the observation volume. Therefore, the number of molecules in the observation volume of a typical FCS experiment is kept small (N $\sim$ 1−10 at $C \sim 10^{-9}$ M) such that a correlation with significant amplitude can be observed. In a calibrated observation volume with an exactly Gaussian profile, $1/e^2$ radial waist r_0, and known ω, the diffusion coefficient D of a fluorescent species can be determined ($D \sim r_0^2/4\tau_D$). However, deviations of the focal volume from the Gaussian assumption are common sources of systematic error that can be eliminated, as discussed in section III.

II.B. Analytic Solution for Multiple Diffusing Species without Chemical Kinetics. For multiple noninteracting fluorescent species ($i = 1, 2, ..., m$) undergoing only diffusion in the observation volume, the overall fluorescence correlation is simply a linear combination of the correlations for each species, weighted by the square of their respective fluorescence intensities (*3*, *26*):

$$G_D(\tau) = \sum_{i=1}^{m}(Q_i\bar{N}_i)^2 G_i(\tau)/(\sum_{i=1}^{m}Q_i\bar{N}_i)^2 = \sum_{i=1}^{m}\bar{F}_i^2 G_i(\tau)/(\sum_{i=1}^{m}\bar{F}_i^2) \qquad (2)$$

where $\bar{F}_i$ and $G_i(\tau)$ are the average fluorescence and autocorrelation for the ith species, respectively, and $Q_i = \sigma_i\varphi_i\psi_i$, where σ_i is the absorption cross section, φ_i is the fluorescence quantum yield, and ψ_i is the detection efficiency. There are limits, however, to the resolution of multiple species. Theoretical and experimental studies on two-component systems in solution (*19*) show that the distinction between two different molecular species depends on differences in their molecular brightness, size, and concentration. Molecules contributing comparably to the total fluorescence must differ in diffusion time by a factor of $\sim$1.6 (i.e., a factor of $\sim$4 difference in hydrodynamic volume for spherical particles) to be distinguished easily.

In addition to diffusion, the concentration fluctuations observed by FCS can be generally attributed to chemical reactions and photoconversion among various molecular electronic states with different fluorescence properties. Accordingly, the analytical form for the autocorrelation function in FCS depends on the fluctuation mechanism, as discussed in section IV.

III. EXPERIMENTAL PROCEDURES

A typical experimental setup (Figure 1a) consists of a high-numerical aperture (NA) objective which focuses a laser beam into the sample (e.g., single cells or solution). The diffraction-limited beam waist in the objective focal plane is on the order of the illumination wavelength λ_x in the lateral dimension (i.e., typically 0.5 μm). Fluorescence is collected through the same objective, separated from the excitation light by both a dichroic mirror and emission filters, and then focused by a tube lens onto a confocal aperture (either an optical fiber or a pinhole) that precedes a detector for depth discrimination. Avalanche photodiodes (APDs) or photomultiplier tubes (PMTs) are usually used for fluorescence detection. Most PMTs tend to have lower quantum efficiencies and a low dark count rate compared to those of APDs, which are highly sensitive but exhibit higher dark count rates. The excitation intensity profile and detection optics (in particular, the confocal aperture) define the $\sim 10^{-15}$ ℓ observation volume (Figure 1b), from which fluorescence photons are detected. The detector signal is then processed with a PC correlator card to calculate the autocorrelation curve (Figure 1c−e). The correlation decay curve is then fitted with an analytic function, which accounts for the mechanism and kinetics of the fluorescence fluctuations. Those processes include translational diffusion of particles through the observation volume (*4*), rotational diffusion within that volume (*5*, *14*, *28*), intersystem crossing (*29*), chemical reactions (*4*, *30*, *31*), conformational fluctuations (*32*, *33*), and photobleaching (*34*−*36*).

Study of numerous molecular processes by FCS requires a high S/N for reliable data analysis. FCS is also susceptible to excitation power instabilities, scattered light, background fluorescence (e.g., impure solvent, cellular autofluorescence), and the statistical limitations of intrinsic photon shot noise. A constant background signal does not correlate; rather, it

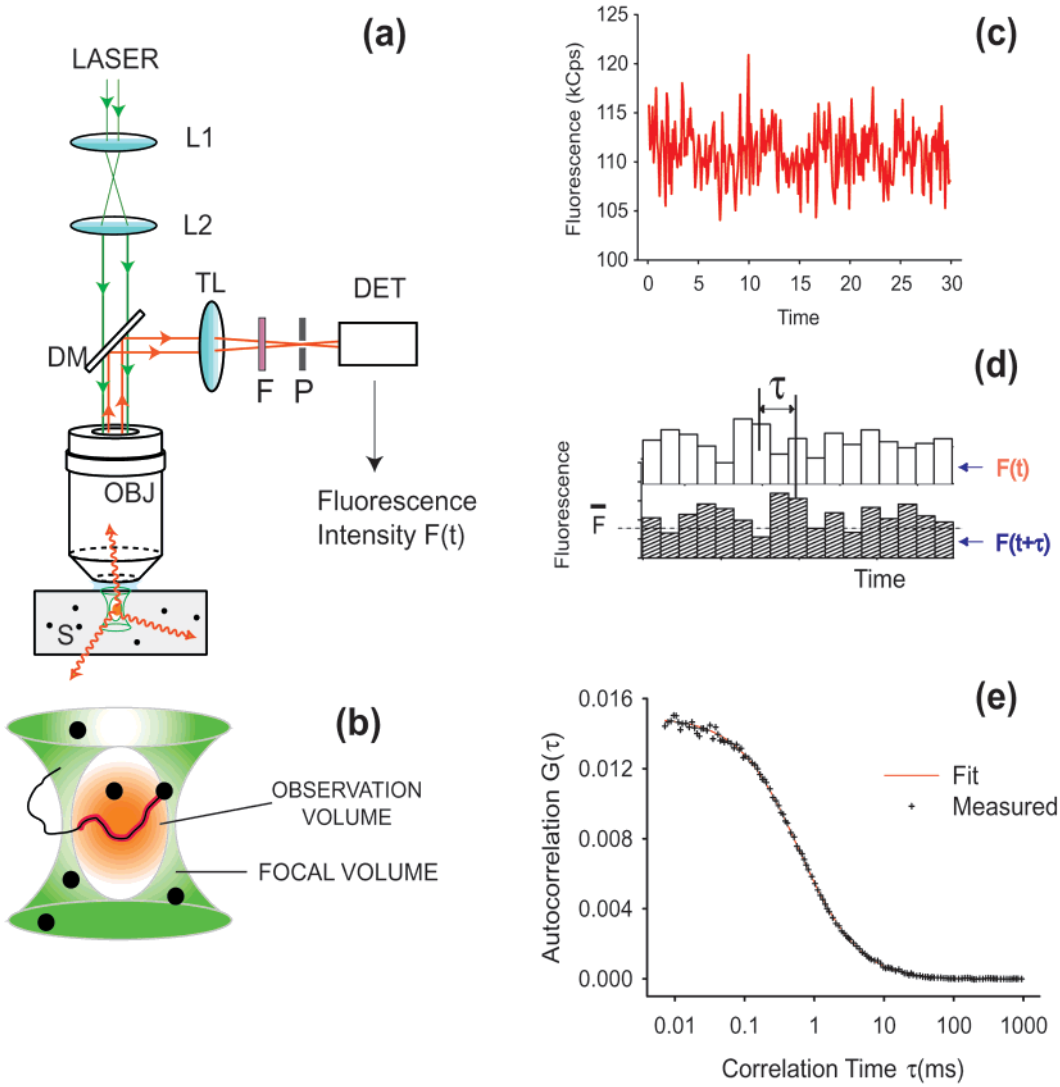

FIGURE 1: (Left) Experimental setup for FCS. (a) A laser beam is first expanded by a telescope (L1 and L2), and then focused by a high-NA objective lens (OBJ) on a fluorescent sample (S). The epifluorescence is collected by the same objective, reflected by a dichroic mirror (DM), focused by a tube lens (TL), filtered (F), and passed through a confocal aperture (P) onto the detector (DET). (b) Magnified focal volume (green) within which the sample particles (black circles) are illuminated. (Right) (c) A typical fluorescence signal, as a function of time, measured for rhodamine green (RG) with a λ_x of 488 nm. (d) Portion of the same signal in panel c, binned, with an expanded time axis and average fluorescence $\bar{F}$. The signal is correlated with itself at a later time ($t + \tau$) to produce the autocorrelation $G(\tau)$. (e) Measured $G(\tau)$ describing the fluorescence fluctuation of RG molecules due to diffusion only as observed by FCS.

affects the correlation function amplitude so that the concentration is overestimated and the count rate per molecule (i.e., molecular brightness) $\eta = \langle F(t)\rangle/N$ is underestimated. In the presence of such background, the measured correlation function amplitude must be scaled by $\langle F(t)\rangle^2/[\langle F(t)\rangle - \langle F_{BG}\rangle]^2$, where $\langle F_{BG}(t)\rangle$ is the time-averaged background signal (*15*). Diffusible background contributes to the correlation as a separate species (see eq 2). To avoid background from contaminated buffer solutions, ultrapure high-pressure liquid chromatography (HPLC) grade water is recommended. Appropriate fluorescence emission filters can minimize background from Raman and hyper-Rayleigh scattering by water. Background contribution, measured using a blank sample, should in general be <5% of the total fluorescence signal. On the other hand, shot noise affects mainly the S/N at short correlation times, where data quality is critical for resolving fast kinetics and estimating the number of molecules. Measuring a correlation on a time scale τ requires detection of at least two photons from the fluctuating entity within a time window τ. If the number of photons per time bin is small (<2), and η cannot be increased, increasing the acquisition time T_m may help, since S/N $\sim \sqrt{T_m}$ (*15*, *16*). Alternately, the S/N in the 100 ns to 10 μs time range can be increased, and systematic errors due to detector afterpulsing can be reduced simultaneously by single-color cross-correlation FCS, in which the fluorescent signal is split between two paths and measured by two detectors simultaneously (*29*).

Another key variable in confocal FCS is detector aperture size, which can drastically affect the S/N (*18*, *37*) and the observation volume. The maximal count rate per molecule (*15*) is obtained with a critical detector aperture diameter (d_0), which depends on the degree of overfilling of the back aperture of the objective, illumination and emission wavelengths, and the objective NA and magnification. An oversized detector aperture (i.e., $d > d_0$) leads to a non-Gaussian observation volume, yielding a correlation curve that cannot be described adequately by eq 1, due to artifacts. Some artifacts are present even with a smaller aperture ($d < d_0$), which can be largely avoided by underfilling the

back aperture of the objective (by ~60%). However, underfilling the objective also results in a larger excitation volume, and hence a larger observation volume and a greater number of observed molecules. Furthermore, both the objective properties and the detector aperture limit the fluorescence collection in confocal FCS. As a result, the fluorescence excited from out-of-focus molecules will not be collected efficiently. Thus, the number of fluorescence photons per second per molecule (i.e., molecular brightness η), a crucial quantity in FCS that determines the S/N, will be lower for an underfilled back aperture. Therefore, a tradeoff has to be made between increasing the S/N and minimizing artifacts by underfilling the objective back aperture.

In a biological environment, observation of multiple fluorescence emitters (or the same emitters in different microenvironments) is common. To ensure accurate data interpretation, the following precautions are recommended. It is essential to measure an autocorrelation curve of a photostable molecule (e.g., rhodamine green) with the lowest possible illumination intensity (with a suitable S/N), as a control. The measured correlation curve needs to be satisfactorily described by eq 1 with a nondivergent structure parameter (ω). A small detector aperture ($d < d_0$) and underfilled (<60%) objective back aperture reduce artifacts to a negligible level for most applications.

Combining 2PE and FCS provides several advantages (*27*, *38*−*40*) over confocal FCS (*39*−*46*), particularly for measurements in cells and tissues. The excitation rate in 2PE depends quadratically on the illumination intensity (*47*) and thus, for a tightly focused beam, declines rapidly with the axial distance (roughly as z^{-4}) from the focal plane. This inherent excitation confinement provides intrinsic 3D spatial resolution and a nearly 3D Gaussian observation volume. Consequently, the detector aperture, used in confocal FCS for depth discrimination, is unnecessary for 2PE-FCS. Confined excitation reduces the level of the background signal, out-of-focus photobleaching, and cellular photodamage. The wide separation between the 2P excitation wavelength and emitted fluorescence allows background due to Raman and Rayleigh scattering of water to be excluded. The 1P absorption of the medium at 2PE wavelengths (700−1000 nm) is usually negligible, so a larger penetration depth is achieved for thick tissue studies even in the presence of intrinsic chromophores (i.e., hemoglobin, myoglobin, and cytochromes). The autocorrelation function for 2PE-FCS is identical to that for ideal confocal FCS, except that the diffusion coefficient D becomes $\sim r_0^2/8\tau_D$, where r_0 is the $1/e^2$ width of the observation profile.

IV. FCS APPLICATIONS IN SOLUTION

The capability of FCS as an analytical tool extends beyond the measurements of molecular concentrations and diffusion times. Kinetic parameters of molecular dynamics or chemical reactions are also accessible when they cause fluorescence fluctuations on time scales faster than the diffusion time. This includes unimolecular reactions, intersystem crossing, triplet state dynamics (*29*, *48*), photoconversion, and reversible photobleaching. However, most biological processes take place on time scales slower than the diffusion time. Such processes include nucleic acid hybridization, ligand-protein binding, and enzyme turnover. Below, we discuss these two categories of applications to assess the potential of FCS in those areas of research, in comparison with conventional methods.

IV.A. Fast Molecular Dynamics: Triplet State and Photobleaching. When chemical kinetics occur on a time scale much faster than the diffusion time τ_D, the dynamics of the m independent transition pathways between a fluorescent state and dark state(s) can be described by (*49*)

$$G(\tau) = G_D(\tau)\prod_{i=1}^{m}\frac{1}{(1-f_i)}(1 - f_i + f_i e^{-\tau/\tau_i}) \qquad (3)$$

The fraction f_i of molecules residing in a dark state[2] for a characteristic time τ_i can be determined from the measurements; for diffusion alone, $f_i = 0$ and $G(\tau) = G_D(\tau)$. The characteristic time (τ_i) of photoconversion between a bright and dark state is the inverse sum of rate constants for the forward (k_F) and reverse (k_R) reactions ($\tau_i^{-1} = k_i = k_F + k_R$). Transitions between bright and dark states (*49*, *50*) resulting from protonation reactions (*49*−*52*), photoconversion, and intersystem crossing (*29*, *34*) have been studied. The presence of dark state transitions also affects the evaluation of the apparent total number of molecules in the observation volume, since $G(0) = N^{-1}$ becomes $G(0) = N^{-1}\prod_{i=1}^{m}(1 - f_i)^{-1}$, which can be used to deduce the number of bright and dark molecules. In molecular systems where $i \geq 2$ (see eq 3), care must be taken both experimentally and in data analysis due to the large number of fitting parameters.

Intensity-dependent FCS measurements can provide valuable information about intersystem crossing dynamics, yielding both the intersystem crossing rate and the triplet state lifetime (typically a few microseconds), useful for designing efficient photosensitizers for photodynamic therapy (*53*), and understanding ground state depletion mechanisms. Triplet states are usually implicated as the gateway to many irreversible photobleaching mechanisms (*54*).

Photobleaching, due to photochemical reactions, removes molecules from the excitation-emission cycle permanently or for a time period longer than the diffusion time in FCS. Excitation intensity-dependent FCS can be used to quantify the photobleaching quantum yield (Φ_b) of a fluorophore (*34*, *35*), where Φ_b is defined as the probability of bleaching a given molecule per excitation. In a typical FCS experiment, molecules can freely diffuse into and out of an open observation volume at a rate $k_D = 1/\tau_D$. However, as the illumination intensity increases, molecules can be photobleached inside the observation volume at a rate $\Phi_b k_x$, where k_x is the excitation rate. The apparent diffusion rate (k_D^a) is dependent on both the excitation rate and the photobleaching quantum yield via the equation $k_D^a = 1/\tau_D^a = k_D + \Phi_b k_x$ (*35*), where k_D^a is generally obtained experimentally by fitting $G(\tau)$ using eq 3 with τ_D replaced by τ_D^a. For example, photobleaching in dsRed is shown as a representative case (Figure 2b,c). In the absence of photobleaching, the apparent diffusion rate $k_D^a = k_D$ and is independent of the illumination intensity (Figure 2b). In the presence of

[2] Molecules in nonabsorbing dark states exit the excitation-emission cycle for an average period of time τ_i, and therefore do not affect the fluorescence quantum yield of the bright state.

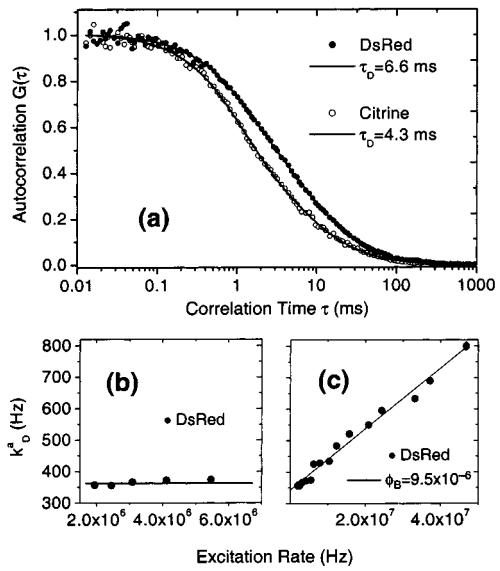

FIGURE 2: Intensity-dependent FCS provides a wealth of information. (a) FCS correlation curves of dsRed (●) and GFP mutant citrine (○) under low-intensity illumination (488 nm, underfilled 1.15 NA 40× water immersion objective, 50 μm detection fiber). The estimated diffusion coefficient D of dsRed (2.6×10^{-11} m^2/s) is smaller than of citrine (4.0×10^{-11} m^2/s), which has the same monomeric molecular weight, indicating an aggregation of dsRed (*49*). The value of $G(0)$ for dsRed yielded $\langle N \rangle = G(0)^{-1} = 74.5$ and concentration $C = \langle N \rangle / V = 74.5/13.0\ \mu\text{m}^3 = 9.5$ nM, which provides an upper bound for the dissociation constant ($K_d \leq 10$ nM) of the dsRed oligomer. (b) The apparent diffusion rate k_D^a ($=1/\tau_D^a$) of dsRed (●) is constant under low-intensity illumination (i.e., low excitation rate). (c) Under high-intensity illumination, however, the diffusion rate increases linearly as a function of excitation rate with a slope equal to the photobleaching quantum yield $\Phi_b = (9.5 \pm 2.0) \times 10^{-6}$.

photobleaching under a high illumination intensity, the apparent diffusion rate increases linearly with the excitation rate and the slope equals $\Phi_b = (\sim 9.5 \pm 0.2) \times 10^{-6}$ for dsRed; see Figure 2c (*50*). To provide a measure of what constitutes high intensity, it is noted that at $k_x \sim 4 \times 10^6$ Hz, the fluorescence signal becomes nonlinear in k_x and eventually approaches a plateau (i.e., saturation) at $k_x \sim 1.5 \times 10^7$ Hz. By conducting such measurements in different environments, one can elucidate the molecular nature of bleaching mechanisms. Furthermore, the average number of fluorescence photons per molecule before bleaching is simply Φ_b^{-1} (i.e., $\sim 1.1 \times 10^5$ for dsRed), an important photophysical parameter for optimal selection of fluorophores.

IV.B. Photoconversion in Green Fluorescent Proteins. Isolation and cloning of GFP (*55*) from the *Aequoria victoria* jellyfish triggered a revolution in fluorescence visualization of gene expression. GFP and many of its mutants can be expressed and targeted to selected cellular compartments with minimal interference with cellular function. Most of these intrinsically fluorescent proteins (IFPs) exhibit both neutral (protonated) and anionic (deprotonated) forms of the embodied chromophore with a pH-sensitive equilibrium partitioning that can be manipulated by site-specific mutagenesis. Thus, many GFPs are pH-sensitive and can be used as intracellular pH indicators. The combination of FCS and GFPs can be an extremely powerful tool for intracellular studies.

GFP is an excellent system for studying protein dynamics by FCS; the protein environment surrounding the chromophore strongly influences its fluorescence properties. Haupts et al. characterized the sub-millisecond fluorescence flicker of EGFP (S65T/F64L) due to external proton exchange with the buffer using FCS (*33*). The reaction rate constants for protonation (3.45×10^9 M^{-1} s^{-1}) and deprotonation (9.05×10^3 s^{-1}) were measured, yielding a pK_a of 5.5 ± 0.3 and a free energy $\Delta_r G^0$ of $\sim$32 kJ/mol. These studies concluded that the hydroxyl group on Tyr66 is the protonation site by comparative studies with the Y66W mutant. Similar studies on T203Y and T203F (*49*) and citrine (*50*) mutants suggest that such protonation reactions are ubiquitous among GFPs. However, for reliable interpretation of intracellular pH measurements using GFPs, calibration under conditions similar to the intracellular environment is required (*51*), and the intensity dependence of the photophysics must be considered to avoid inaccuracy (see below).

Recent studies on the photophysics of another IFP, dsRed (from a coral of the *Discosoma* genus) (*50*), showed pH-independent autocorrelation over the pH range of 3.9−11. Remarkably, the amino acid sequences of dsRed and wild-type GFP are somewhat similar, despite their different origins, and their X-ray crystal structures are strikingly similar (*56*). However, in contrast to GFPs, dsRed forms a stable tetramer (Figure 2a) with a dissociation constant k_d of $\leq$10 nM, as revealed by FCS (*50*), fluorescence anisotropy (*50*), and electrophoresis (*57*).

Light-driven fluorescence flicker is another common feature of IFPs. In addition to flicker due to reversible external protonation in EGFP, an excitation intensity-dependent flicker was observed (with dynamics independent of pH) with a mean dark fraction of $\sim$13% (*33*), complicating the interpretation of intracellular pH measurements. Furthermore, a slow ($\sim$1 s) light-dependent fluorescence blinking of immobilized individual T203Y and T203F proteins at a low illumination intensity was reported (*52*) using wide-field fluorescence microscopy. The on/off switching is excitation wavelength-dependent due to photoconversion among the anionic, intermediate, and neutral states of the chromophore (*52*). These findings triggered FCS studies on these mutants (*49*), as well as citrine (*50*), which revealed fast ($\sim$10−100 kHz) intensity- and pH-dependent flicker. Similar findings in dsRed suggest that intensity-driven fluorescence flicker is widespread among IFPs (*58*).

FCS has also been used to study FRET between the fluorescently labeled ends of DNA hairpin loops as they fluctuate between open and closed structures (*32*). These "molecular beacons" show promise as a sensitive hybridization-based sparse molecule DNA assay, of great interest for biosensor development and basic research.

IV.C. Intermolecular Interactions in Heterogeneous Systems. Many biological systems of interest are heterogeneous mixtures of fluorescent species of different sizes and fluorescence properties. The correlation curve of multiple noninteracting diffusing species is a linear combination of contributions from each species (see eq 2). Numerous FCS applications focus on molecular interactions resulting in large changes in hydrodynamic volume, such as those between ligand and receptor, peptide and liposome, or a DNA primer and a large complementary DNA or RNA strand.

Nucleic Acids. Nucleic acids can be site-specifically labeled with fluorescent probes with minimal effect on their hybridization. At nanomolar concentrations, which are orders

of magnitude lower than those used in traditional fluorescence methods such as FRET (*59*), some slow hybridization reaction kinetics can be followed by performing serial FCS measurements. Exploiting these advantages, the kinetics of association of fluorescently labeled DNA primers to large DNA or RNA molecules have been examined as a function of temperature (*60*) or RNA secondary structure (*61*). These studies demonstrate that FCS sensitivity is comparable to that of radioactive assays, but without the burdensome requirements for radioactive materials and physical separation of reactive species. Also, compared to CD (circular dichroism) spectroscopy and calorimetry for monitoring hybridization reactions, FCS requires significantly less sample and provides information about molecular diffusion, brightness, aggregation, sample concentration, and chemical and conformational kinetics.

The ultrasensitive detection of viral and bacterial pathogens (*62*−*64*) is another cogent biological application of FCS. Pathogen-specific DNA or RNA sequences were amplified using various forms of polymerase chain reaction (PCR), during which fluorescently labeled primers at 1−5 nM and unlabeled primers were incorporated into the extended PCR products. The transition from fast-diffusing primer to slow-diffusing product was monitored and quantified by FCS as a function of PCR amplification cycles, and then used to deduce initial pathogen concentrations. FCS has been utilized for detecting HIV-1 RNA and *Mycobacterium tuberculosis* DNA mixed with high concentrations of nonspecific DNA background (*62*, *63*), where the false-positive detection frequency was significantly reduced. Furthermore, *in situ* FCS monitoring during PCR amplification eliminates the lengthy procedures of post-PCR product identification as well as carryover contamination risks (*62*). FCS has also been used to detect sub-nanomolar β-amyloid protein aggregates in cerebrospinal fluid of Alzheimer's disease patients (*65*).

Micelles and Liposomes. In early studies, Koppel et al. (*7*) used FCS to measure the sizes of micelles formed by amphiphilic carbocyanine dyes [*66*, *67*; see also Herbert et al. as reported by Webb (*11*)]. Recently, FCS has been applied to protein and peptide interactions with liposomes. Because such interactions yield large changes in diffusion correlation times (*68*−*70*), resolution of multiple species and their properties can be carried out using FCS as well as QELS. Measurements of vesicle and micelle hydrodynamic volume using both techniques have been demonstrated to be equivalent (*71*−*73*). However, the concentration sensitivity of FCS is orders of magnitude higher than that of QELS and is thereby able to determine extremely low critical micelle concentrations by measuring the diffusion correlation times as a function of detergent concentration (*72*). Both FCS and time-resolved fluorescence anisotropy (TRFA) are used to derive dynamic information from micelles and liposomes, albeit at different time scales (*71*). However, TRFA is limited by the excited state fluorescence lifetime (a few nanoseconds) of the labels and thus is suitable primarily for studying fast dynamics influenced by the local lipid environment. On the other hand, FCS readily resolves dynamic processes ranging from the microsecond to ~1 s time range, and therefore is a superior method for measuring hydrodynamic volumes of large liposomes and micelles.

Protein-Protein and Ligand-Receptor Interactions. Protein-protein and protein-ligand interactions with sub-micromolar binding affinities are well-suited for FCS studies. For example, the dimerization process of the δ-subunit of ATP synthase (*74*) has a K_d of <0.2 nM, as determined by FCS. When the competing dimerization process is considered, results show that the free energy of δ-subunit binding to the headpiece of the enzyme is large enough to withstand the torque expected from the three-step conformational change during ATP synthesis. Such a high-affinity process was invisible to TRFA measurements, which require sample concentrations of >1 μM. Furthermore, from differences in the free and bound ligand concentrations as a function of receptor concentration, the binding stoichiometry can be determined by FCS (*37*, *75*). In addition, pseudo-first-order kinetics are resolved under conditions where the receptor concentrations are much higher than those of fluorescently labeled ligands (*76*, *77*). However, the ~1 nM concentration of fluorescent molecules required for FCS can be a limiting factor in the study of enzymatic mechanisms, where the physiological substrate affinity is usually much higher (i.e., approximately micromolar). In an attempt to circumvent this limitation, Meyer-Almes and Auer (*78*) have proposed a new analytical method that can recover Michaelis-Menten constants at nanomolar substrate and enzyme concentrations. A second concern is the possibility that a fluorescent label might disrupt the ligand-receptor interaction (*79*), which is often resolved by choosing an appropriate fluorescent dye bound at a minimally disruptive labeling site. Alternately, competitive binding studies using unlabeled versus labeled ligand (*74*, *75*) can be used to test whether the label affects the apparent K_d. Despite these complications, FCS has demonstrated its versatility for studying a variety of protein-protein and protein-ligand systems (*76*−*83*).

Recent developments in FCS methods have improved its ability to assess binding reactions between similarly sized molecules. Dual-color FCS (*84*) cross-correlates the fluorescence signals registered on separate detectors from two species with distinct emission spectra. The cross-correlation amplitude corresponds directly to the concentration of the reaction product that bears both fluorescence signals. Kinetics of DNA renaturation (*84*), DNA cleavage by restriction enzymes (*85*), and transcription activator protein-DNA binding (*86*) have been successfully studied using this method. In principle, any reactions that facilitate or disrupt the association of two fluorescent labels can be monitored by dual-color FCS. This technique is further enhanced by using 2PE, where excitation of both labels can be achieved with a single 2PE wavelength (*40*), eliminating the technical difficulty of aligning two observation volumes in 1PE dual-color FCS.

IV.D. New Methods for Resolving Multiple Species. Recently, the photon counting histogram (PCH) (*22*, *87*) and fluorescence intensity distribution analysis (FIDA) (*88*, *89*), which use the same experimental geometry that is used in FCS, have gained ground as new approaches to fluorescence fluctuation analysis. While the autocorrelation describes the temporal evolution of fluorescence fluctuations, PCH and FIDA measure the probability distribution of fluorescence fluctuations as a function of amplitude. These new techniques have been applied to study the binding of a fluorescent ligand to a protein with single- and double-site binding selectivity

(*22*, *90*). Of particular interest is the utilization of FIDA for high-throughput screening by pharmaceutical companies, with detection sensitivity to femtomolar concentrations of fluorescently labeled aggregates such as prion protein (*91*). Fluorescent photons can also be gated, on the basis of the excited fluorescence lifetime of fluorescent labels, prior to autocorrelation (*92*). Advances in single-molecule fluorescence observation technology (*93*−*95*) now combine FCS and a number of other techniques (i.e., FIDA, fluorescence lifetime, and spectral gating) for a proposed high-throughput screening (HTS) of $\sim 10^5$ samples per day in mixtures of multiple species with similar diffusion coefficients (*96*−*98*). Such FCS-HTS assays have the advantage over FRET-based HTS methods since the labeling sites of the two fluorescent dyes are not limited by the distance separating them.

V. CELLULAR APPLICATIONS OF FCS

The first successful FCS measurements in cell membranes were reported by Elson et al. (*66*). However, FCS measurements within cells are susceptible to interference from autofluorescence and perturbations due to cellular photodamage and photobleaching (*38*, *39*). 2PE minimizes these problems and provides accurate FCS in living cells (*39*). It is known that NADH and flavoproteins, mostly localized in the cellular mitochondria, are two main sources of autofluorescence. The contribution of autofluorescence in cellular FCS can be minimized by careful selection of fluorescent labels. Since NADH and flavoproteins have typically low fluorescence quantum yields and are easily photobleached, their signal will not correlate efficiently if each fluorophore contributes on average <1 detectable photon during its diffusion through the observation volume. In this case, the presence of autofluorescence may affect the amplitude of the correlation curve (i.e., N) but not its decay parameters (*39*), and can be corrected for as a constant background (see section III). Immobilized intrinsic fluorescence is typically photobleached sufficiently rapidly that its contribution to the FCS signal is negligible (*39*).

V.A. Cellular Membranes. Membranes are the gatekeepers for many important cellular functions and often have negligible autofluorescence, making them a favorable environment for cellular FCS. The thickness of the lipid bilayer ($\sim$4 nm) is 3 orders of magnitude smaller than the typical axial length of the FCS observation volume ($\sim 1\ \mu$m), and therefore, the diffusion of a fluorescent label in the membrane can be treated as two-dimensional (see section II). Early applications of FCS for membrane applications in the 1970s included model membrane systems such as planar lipid bilayer membranes (*7*, *10*, *11*, *67*). Similar FCS measurements were first extended to the membranes of living cells and compared with FPR results by Elson et al. (*66*). Recently, the phase segregation patterns and equilibrium coexistence properties in various lipid mixtures were examined by a combination of FCS and laser scanning microscopy (*44*, *99*). The estimated diffusion coefficients agree with those measured by FPR. Giant unilamellar vesicles (GUVs) doped with lipophilic dyes were used to study lipid phase separation (*44*, *99*). Simple diffusion was found to be insufficient to describe the observed correlation curves on either GUVs undergoing phase transition or actual cell membranes. Assuming anomalous subdiffusion (*100*), or a sum of two diffusing species, improved the fitting residuals. On the other hand, while the anomalous subdiffusion model might answer many interesting biological questions, distinction between an anomalous subdiffusion model and superposition of several diffusing species is often difficult and would likely benefit from further investigation.

V.B. Ligand-Membrane Receptor Interactions. Understanding the mechanisms of ligand-membrane receptor interactions in their native environment is essential for developing therapeutic reagents (*101*). However, the scarcity of these molecules in their physiological environment and their high-affinity (i.e., $K_d \leq 10$ nM) interactions had typically required radioactive assays. Now, FCS is easily used to monitor molecules at nanomolar concentrations, and can be carried out on cell surfaces (*45*). Ligand-membrane receptor interaction studies were initially carried out using FCS *in vitro*, where receptor proteins were solubilized in detergent (*31*, *75*, *77*), and the estimated binding constants were found to be comparable to those derived from radioactive assays. For ligand-receptor binding on membrane surfaces of single cells (*45*), a relatively large observation volume was used, which simultaneously detected 2D and 3D diffusion of the fluorescently labeled proinsulin C peptide in the cell membrane and in the extracellular space. Subnanomolar binding affinities were then determined for several types of cultured human cells, and the receptor-mediated binding specificity was established through competitive displacement and drug inhibition studies.

V.C. Intracellular Compartments. Compartments of the cytosol and nucleus have been explored on the single-cell level using FCS. Politz et al. examined diffusion and hybridization of nucleotides within the nucleus of cultured rat myoblasts (*43*). As expected, fitting parameters derived from FCS measurements of intracellular compartments reflect properties of a highly heterogeneous microenvironment (*42*, *43*, *102*). Understanding such heterogeneity and the ability to resolve molecular properties within single cells will contribute significantly to the understanding of biological processes. For example, the high cooperativity of the chemotactic pathway in *Escherichia coli* would have been averaged out in ensemble measurements if not for the capability of FCS to measure the concentration of signaling molecules in single cells (*46*).

Cellular studies within the physiological environment represent a challenge that can be met by FCS, considering its sensitivity and spatial and temporal resolution. However, the foundation for such experiments needs further attention. Gennerich and Schild (*103*) have examined a situation where the fluorescent marker distribution was restricted to cellular compartments, demonstrating the complexity involved in FCS data analysis. If care is taken to address the complexity of intracellular studies, FCS can be an invaluable tool for single-cell studies.

VI. FUTURE PERSPECTIVE

Advances in hardware, software, and fluorescent markers continue to open new avenues for FCS applications in biology and chemistry. Volume confinement schemes which combine FCS with surface-enhanced excitation (*104*) or optical nanostructures for sample confinement (*105*; J. Korlach et al., unpublished results) may provide access to higher ($>1\ \mu$M) concentrations for FCS and better resolution

of subcellular structures. Nanostructured channels have already proven to be useful in fast (microsecond to millisecond) mixing experiments for biological studies such as protein folding (*106*). Detectors with enhanced quantum efficiency and low dark counts will further improve single-molecule and FCS studies. Current 1P-FCS microscope systems detect less than ~5% of the emitted fluorescence, with a significant loss due to the required confocal pinhole. Optimized integrating optical geometries may significantly improve the detection efficiency. The combination of MPE-FCS and scanning microscopy using detectors with a wide (>300 μm) active surface is advantageous for simultaneous imaging and site-specific FCS. Because of the confined excitation volume in FCS, a very stable excitation beam during measurements is crucial, but remains a nontrivial problem to overcome in laser scanning microscopy (LSM). Fortunately, preliminary control experiments (D. Larson et al., personal communication) show that beam jitter can be avoided; for example, in a Bio-Rad MRC-600 adapted 2PE-LSM, beam jitter is not a problem. FCS-FIDA may also be possible in a circular or oscillatory scanning mode (*107*), which would decrease the residence time of a given molecule in the excitation volume, minimize ground state depletion, and potentially increase molecular brightness. Finally, ultrafast correlator cards and detectors with picosecond transient times can expand the temporal domain for FCS applications to a broader spectrum of chemical and biological processes.

REFERENCES

1. Magde, D., Elson, E., and Webb, W. W. (1972) *Phys. Rev. Lett. 29*, 705.
2. Cummins, H. Z., and Swinney, H. L. (1970) *Prog. Opt. 8*, 135.
3. Elson, E. L., and Magde, D. (1974) *Biopolymers 13*, 1.
4. Magde, D., Elson, E., and Webb, W. W. (1974) *Biopolymers 13*, 29.
5. Ehrenberg, M., and Rigler, R. (1974) *Chem. Phys. 4*, 390.
6. Magde, D., Webb, W. W., and Elson, E. (1978) *Biopolymers 17*, 361.
7. Koppel, D. E., Axelrod, D., Schlessinger, J., Elson, E. L., and Webb, W. W. (1976) *Biophys. J. 16*, 1315.
8. Ehrenberg, M., and Rigler, R. (1976) *Q. Rev. Biophys. 9*, 69.
9. Aragón, S. R., and Pecora, R. (1975) *Biopolymers 14*, 119.
10. Fahey, P. F., Koppel, D. E., Barak, L. S., Wolf, D. E., Elson, E. L., and Webb, W. W. (1977) *Science 195*, 305.
11. Webb, W. W. (1976) *Q. Rev. Biophys. 9*, 49.
12. Eigen, M., and Rigler, R. (1994) Sorting single molecules: Application to diagnostics and evolutionary biotechnology, *Proc. Natl. Acad. Sci. U.S.A. 91*, 5740.
13. Maiti, S., Haupts, U., and Webb, W. W. (1997) *Proc. Natl. Acad. Sci. U.S.A. 94*, 11753.
14. Aragón, S. R., and Pecora, R. (1976) *J. Chem. Phys. 64*, 1791.
15. Koppel, D. E. (1974) *Phys. Rev. A 10*, 1938.
16. Kask, P., Günther, R., and Axhausen, P. (1997) *Eur. Biophys. J. 25*, 163.
17. Qian, H. (1990) *Biophys. Chem. 38*, 49.
18. Rigler, R., Mets, U., Widengren, J., and Kask, P. (1993) *Eur. Biophys. J. 22*, 169.
19. Meseth, U., Wohland, T., Rigler, R., and Vogel, H. (1999) *Biophys. J. 76*, 1619.
20. Kask, P., Palo, K., Ullmann, D., and Gall, K. (1999) *Proc. Natl. Acad. Sci. U.S.A. 96*, 13756.
21. Chen, Y., Müller, J. D., So, P. T. C., and Gratton, E. (1999) *Biophys. J. 77*, 553.
22. Chen, Y., Müller, J. D., Tetin, S. Y., Tyner, J. D., and Gratton, E. (2000) *Biophys. J. 79*, 1074.
23. Webb, W. W. (2001) in *Fluorescence Correlation Spectroscopy Theory and Applications* (Rigler, R., and Elson, E. S., Eds.) pp 305−330, Springer-Verlag, Berlin.
24. Onsager, L. (1931) *Phys. Rev. 37*, 405.
25. Webb, W. W. (2001) *Appl. Opt. 40*, 3969.
26. Thompson, N. L. (1991) in *Topics in Fluorescence Spectroscopy* (Lakowicz, J. R., Ed.) Vol. 1, pp 337−410, Plenum Press, New York.
27. Denk, W., Strickler, J. H., and Webb, W. W. (1990) *Science 248*, 73.
28. Kask, P., Piksarv, P., Poogma, M., Mets, U., and Lippman, E. (1989) *Biophys. J. 55*, 213.
29. Widengren, J., Mets, U., and Rigler, R. (1995) *J. Phys. Chem. 99*, 13368.
30. Magde, D. (1976) *Q. Rev. Biophys. 9*, 35.
31. Rauer, B., Neumann, E., Widengren, J., and Rigler, R. (1996) *Biophys. Chem. 58*, 3.
32. Bonnet, G., Krichevsky, O., and Libchaber, A. (1998) *Proc. Natl. Acad. Sci. U.S.A. 95*, 8602.
33. Haupts, U., Maiti, S., Schwille, P., and Webb, W. W. (1998) *Proc. Natl. Acad. Sci. U.S.A. 95*, 13573.
34. Widengren, J., and Rigler, R. (1996) *Bioimaging 4*, 149.
35. Mertz, J. (1998) *Eur. Phys. J. 3*, 53.
36. Eggeling, C., Widengren, J., Rigler, R., and Seidel, C. A. M. (1998) *Anal. Chem. 70*, 2651.
37. Qian, H., and Elson, E. L. (1991) *Appl. Opt. 30*, 1185.
38. Berland, K. M., So, T. C., and Gratton, E. (1995) *Biophys. J. 68*, 694.
39. Schwille, P., Haupts, U., Maiti, S., and Webb, W. W. (1999) *Biophys. J. 77*, 2251.
40. Heinze, K. G., Kolterman, A., and Schwille, P. (2000) *Proc. Natl. Acad. Sci. U.S.A. 97*, 10377.
41. Brock, R., Hink, M. A., and Jovin, T. M. (1998) *Biophys. J. 75*, 2547.
42. Brock, R., Vàmosi, C., Vereb, G., and Jovin, T. M. (1999) *Proc. Natl. Acad. Sci. U.S.A. 96*, 10123.
43. Politz, J. C., Browne, E. S., Wolf, D. E., and Pederson, T. (1998) *Proc. Natl. Acad. Sci. U.S.A. 95*, 6043.
44. Schwille, P., Korlach, J., and Webb, W. W. (1999) *Cytometry 36*, 176.
45. Rigler, R., Pramanik, A., Jonasson, P., Kratz, G., Jansson, O. T., Nygren, P.-Å., Ståhl, S., Ekberg, K., Johansson, B.-L., Uhlén, S., Uhlén, M., Jörnvall, H., and Wahren, J. (1999) *Proc. Natl. Acad. Sci. U.S.A. 96*, 13318.
46. Cluzel, P., Surette, M., and Leibler, S. (2000) *Science 287*, 1652.
47. Xu, C., and Webb, W. W. (1997) in *Topics in Fluorescence Spectroscopy* (Lakowicz, J. R., Ed.) Vol. 5, pp 471−540, Plenum Press, New York.
48. Lakowicz, J. R. (1999) *Principles of Fluorescence Spectroscopy*, 2nd ed., p 5, Kluwer Academic/Plenum Press, New York.
49. Schwille, P., Kummer, S., Heikal, A. A., Moerner, W. E., and Webb, W. W. (2000) *Proc. Natl. Acad. Sci. U.S.A. 97*, 151.
50. Heikal, A. A., Hess, S. T., Baird, G. S., Tsien, R. Y., and Webb, W. W. (2000) *Proc. Natl. Acad. Sci. U.S.A. 97*, 11996.
51. Widengren, J., Terry, B., and Rigler, R. (1999) *Chem. Phys. 249*, 259.
52. Dickson, R. M., Cubitt, A. B., Tsien, R. Y., and Moerner, W. E. (1997) *Nature 388*, 355.
53. Moor, A. C. E. (2000) *J. Photochem. Photobiol. B 57*, 1.
54. Molski, A. (2001) *J. Chem. Phys. 114*, 1142.
55. Tsien, R. Y. (1998) *Annu. Rev. Biochem. 67*, 509.
56. Yarbrough, D., Wachter, R. M., Kallio, K., Matz, M. V., and Remington, S. J. (2001) *Proc. Natl. Acad. Sci. U.S.A. 98*, 462.
57. Baird, G. S., Zacharias, D. A., and Tsien, R. Y. (2000) *Proc. Natl. Acad. Sci. U.S.A. 97*, 11984.
58. Malvezzi-Campeggi, F., Jahnz, M., Heinze, K. G., Dittrich, P., and Schwille, P. (2001) *Biophys. J. 81*, 1776.
59. Morrison, L. E., and Stols, L. M. (1993) *Biochemistry 32*, 3095.
60. Kinjo, M., and Rigler, R. (1995) *Nucleic Acids Res. 23*, 1795.
61. Schwille, P., Oehlenschläger, F., and Walter, N. G. (1996) *Biochemistry 35*, 10182.

62. Oehlenschläger, F., Schwille, P., and Eigen, M. (1996) *Proc. Natl. Acad. Sci. U.S.A. 93*, 12811.
63. Walter, N. S., Schwille, P., and Eigen, M. (1996) *Proc. Natl. Acad. Sci. U.S.A. 93*, 12805.
64. Schwille, P., Bieschke, J., and Oehlenschläger, F. (1997) *Biophys. Chem. 66*, 211.
65. Pitschke, M., Prior, R., Haupt, M., and Riesner, D. (1998) *Nat. Med. 4*, 832.
66. Elson, E. L., Schlessinger, J., Koppel, D. E., Axelrod, D., and Webb, W. W. (1976) in *Measurement of Lateral Transport on Cell Surfaces* (Marchesi, V. T., Ed.) pp 137−140, Alan R. Liss, Inc., New York.
67. Wolf, D. E., Schlessinger, J., Elson, E. L., Webb, W. W., Blumenthal, R., and Henkart, P. (1977) *Biochemistry 16*, 3476.
68. Dorn, I. T., Neumaier, K. R., and Tamp, R. (1998) *J. Am. Chem. Soc. 120*, 2753.
69. Takakuwa, Y., Pack, C.-G., An, X.-Li., Manno, S., Ito, E., and Kinjo, M. (1999) *Biophys. Chem. 82*, 149.
70. Pramanik, A., Thyberg, P., and Rigler, R. (2000) *Chem. Phys. Lipids 104*, 35.
71. Hink, M. A., van Hoek, A., and Visser, A. J. W. G. (1999) *Langmuir 15*, 992.
72. Schuch, H., Klingler, J., Rossmanith, P., Frechen, T., Gerst, M., Feldthusen, J., and Müller, A. H. E. (2000) *Macromolecules 33*, 1734.
73. Borst, J. W., Visser, N. V., Kouptsova, O., and Visser, A. J. W. G. (2000) *Biochim. Biophys. Acta 1487*, 61.
74. Häsler, K., Pänke, O., and Junge, W. (1999) *Biochemistry 38*, 13759.
75. Wohland, H., Friedrich, K., Hovius, R., and Vogel, H. (1999) *Biochemistry 38*, 8671.
76. Meyer-Almes, F.-J., Wyzgol, K., and Powell, M. J. (1998) *Biophys. Chem. 75*, 151.
77. Schüler, J., Frank, J., Trier, U., Schäfer-Korting, M., and Saenger, W. (1999) *Biochemistry 38*, 8402.
78. Meyer-Almes, F.-J., and Auer, M. (2000) *Biochemistry 39*, 13261.
79. Van Craenenbroeck, E., and Engelborghs, Y. (1999) *Biochemistry 38*, 5082.
80. Klingler, J., and Friedrich, T. (1997) *Biophys. J. 73*, 2195.
81. Sevenich, F. W., Langowski, J., Weiss, V., and Rippe, K. (1998) *Nucleic Acids Res. 26*, 1373.
82. Tjernberg, L. O., Pramanik, A., Björling, S., Thyberg, P., Thyberg, J., Nordstedt, C., Berndt, K. D., Terenius, L., and Rigler, R. (1998) *Chem. Biol. 6*, 53.
83. Pack, C.-G., Aoki, K., Taguchi, H., Yoshida, M., Kinjo, M., and Tamura, M. (2000) *Biochem. Biophys. Res. Commun. 267*, 300.
84. Schwille, P., Meyer-Almes, F.-J., and Rigler, R. (1997) *Biophys. J. 72*, 1878.
85. Kettling, U., Koltermann, A., Schwille, P., and Eigen, M. (1998) *Proc. Natl. Acad. Sci. U.S.A. 95*, 1416.
86. Rippe, K. (2000) *Biochemistry 39*, 2131.
87. Eid, J. S., Müller, J. D., and Gratton, E. (2000) *Rev. Sci. Instrum. 71*, 361.
88. Kask, P., Palo, K., Fay, N., Brand, L., Mets, U., Ullmann, D., Jungmann, J., Pschorr, J., and Gall, K. (2000) *Biophys. J. 78*, 1703.
89. Kask, P., Palo, K., Ullmann, D., and Gall, K. (1999) *Proc. Natl. Acad. Sci. U.S.A. 96*, 13756.
90. Müller, J. D., Chen, Y., and Gratton, E. (2000) *Biophys. J. 78*, 474.
91. Bieschke, J., Giese, A., Schulz-Schaeffer, W., Zerr, I., Poser, S., Eigen, M., and Kretzschmar, H. (2000) *Proc. Natl. Acad. Sci. U.S.A. 96*, 5468.
92. Lamb, D. C., Schenk, A., Röcker, C., Scalfi-Happ, C., and Nienhaus, G. U. (2000) *Biophys. J. 79*, 1129.
93. Prummer, M., Hübner, C. G., Sick, B., Hecht, B., Renn, A., and Wild, U. P. (2000) *Anal. Chem. 72*, 443.
94. Fries, J. R., Brand, L., Eggeling, C., Kollner, M., and Seidel, C. A. M. (1998) *J. Phys. Chem. A 102*, 6601.
95. Eggeling, C., Fries, J. R., Brand, L., Gunther, R., and Seidel, C. A. M. (1998) *Proc. Natl. Acad. Sci. U.S.A. 95*, 1556.
96. Koltermann, A., Kettling, U., Bieschke, J., Winkler, T., and Eigen, M. (1998) *Proc. Natl. Acad. Sci. U.S.A. 95*, 1421.
97. Winkler, T., Kettling, U., Koltermann, A., and Eigen, M. (1999) *Proc. Natl. Acad. Sci. U.S.A. 96*, 1375.
98. Brinkmeier, M., Dorre, K., Stephan, J., and Eigen, M. (1999) *Anal. Chem. 71*, 609.
99. Korlach, J., Schwille, P., Webb, W. W., and Feigenson, G. W. (1999) *Proc. Natl. Acad. Sci. U.S.A. 96*, 8461.
100. Feder, T. J., Brust-Mascher, I., Slattery, J. P., Baird, B., and Webb, W. W. (1996) *Biophys. J. 70*, 2767.
101. Hubbard, R. E. (1999) *Curr. Opin. Biotechnol. 8*, 696.
102. Kohler, R. H., Schwille, P., Webb, W. W., and Hanson, M. R. (2000) *J. Cell Sci. 113*, 3921.
103. Gennerich, A., and Schild, D. (2000) *Biophys. J. 79*, 3294.
104. Kawata, Y., Xu, C., and Denk, W. (1999) *J. Appl. Phys. 85*, 1294.
105. Levene, M., Larson, D., Korlach, J., Foquet, M., Turner, S. W., Craighead, H. G., and Webb, W. W. (2000) *Biophys. J. 78*, 2368.
106. Pollack, L., Tate, M. W., Darnton, N. C., Knight, J. B., Gruner, S. M., Eaton, W. A., and Austin, R. H. (1999) *Proc. Natl. Acad. Sci. U.S.A. 96*, 10115.
107. Chen, Y., Mueller, J., and Gratton, E. (2000) *Biophys. J. 78*, 2603.

BI0118512